

Imaging the Wairarapa Fault at Tauwharenikau using magnetotelluric sounding

OLAF INGO VON BORSTEL

School of Earth Sciences
Victoria University of Wellington
P.O. Box 600
Wellington, New Zealand*

MALCOLM INGHAM

School of Chemical & Physical Sciences
Victoria University of Wellington

*Present address: Astrophysical Institute and University
Observatory, Friedrich Schiller University Jena,
Schillergaesschen 2, 07745 Jena, Germany.

Abstract To test the ability of closely spaced magnetotelluric data to provide high resolution images of fault structures, measurements have been made across the Wairarapa Fault at Tauwharenikau, southern North Island, New Zealand. 2D inversion and modelling of the TM-mode data from 11 sites on a 1.5 km long transect show the transition from conductive Tertiary sediments southeast of the fault zone to resistive greywacke to the northwest, and also illustrate some of the difficulties in interpretation that can arise. The existence of dual fault traces separated by some 100 m allows for two possible interpretations of the electrical structure: (1) that the southeastern fault trace represents the main trace of the Wairarapa Fault and that low resistivity to the northwest is the result of fluid percolation into fractured rock between the fault traces; or (2) that the northwestern fault trace marks the actual contact between Tertiary sediments and greywacke. In this case, the near-surface dip of the fault is constrained to be c. 80° to the northwest.

Keywords magnetotelluric sounding; Wairarapa Fault; New Zealand

INTRODUCTION

Electrical and electromagnetic geophysical techniques have been used in studies of fault zones in various parts of the world (e.g., Schnegg et al. 1983, 1986; Jones et al. 1992; Ingham & Brown 1998; Unsworth et al. 1999). Such studies have generally been concerned with major transform or strike-slip faults and have been sensitive to the occurrence of low electrical resistivity (often resulting from the presence

of fluids) within the fault zone. The primary importance of these studies is the accumulated evidence that suggests that fluids play an important role in a variety of faulting processes (e.g., Sibson et al. 1988; Rice 1992; Hickman et al. 1995; Crampin et al. 2002). The typical spacing of measurement sites in such investigations is of the order of a few hundred metres, and this has proved sufficient to produce images of lateral variations in structure occurring over a similar scale. However, model studies (Ingham in press) suggest that more closely spaced measurements may be able to provide even more highly detailed images of fault zones. This suggests not only improved resolution of the presence of fluids within a transform fault zone, but, in normal or thrust faults where a significant electrical resistivity contrast exists across the fault, might also enable determination of the dip of the fault.

We report here the results of a study designed primarily to provide a field test of the ability of closely spaced electromagnetic data to provide such high resolution images of the electrical structure of a fault. The study uses closely spaced magnetotelluric (MT) measurements made across the Wairarapa Fault in the North Island of New Zealand (Fig. 1).

MT SOUNDINGS

MT measurements were made at 11 locations on a 1.5 km long transect of the Wairarapa Fault where it cuts across the Tauwharenikau River valley (Fig. 1). The surface structure of the Wairarapa Fault in this vicinity has been described in detail by Grapes & Wellman (1988). Northeast of the river, two fault traces are separated by c. 100 m. The major fault scarp is associated with the southeastern fault trace and is downthrown to the southeast. At the location of the MT transect a shallow trough has formed between the fault traces, which Grapes & Wellman (1988) attributed to either gravity collapse during earthquake shaking or a dextral offset of c. 20 m on the main fault trace to the northeast.

Seven soundings, at separations of only 50 or 75 m, were carried out across the fault zone itself (Fig. 1). The other four soundings were at greater separations on either side of the fault zone. Measurements of time variations in horizontal components of the naturally occurring magnetic and electric fields were made over a nominal frequency range of 300–0.3 Hz in an axial system oriented perpendicular and parallel to the observed fault zone. In the chosen axial system, assuming the electrical structure associated with the fault is 2D, the off-diagonal elements of the impedance tensor, relating to the electric field perpendicular and parallel to the fault, should correspond to the impedances associated with the transverse magnetic (TM) and transverse electric (TE) modes of electromagnetic induction, respectively. In general, the TM mode impedance exhibits a much sharper spatial response to changes in electrical resistivity across a boundary than does the TE impedance. For this reason, lateral changes in resistivity across a geological structure are often derived

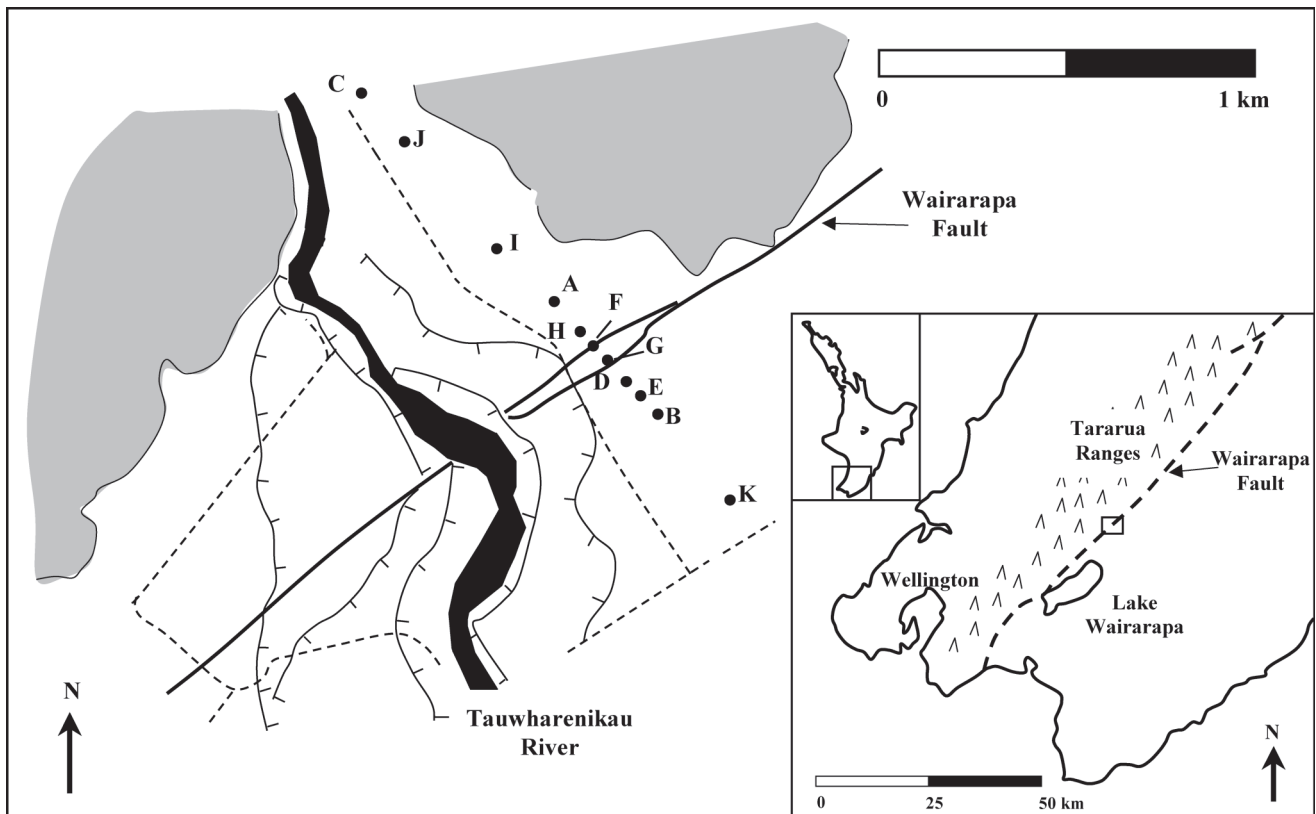


Fig. 1 Location of the Wairarapa Fault and MT sites adjacent to the Tauwharenikau River in the southern part of the North Island of New Zealand. Dashed lines are public and farm roads. Thin lines represent the edges of river terraces. Grey shading indicates higher topography where basement greywacke of the Tararua Ranges is exposed through the surface cover of Quaternary gravels.

from solely the TM mode impedance (Wannamaker 1999). In addition, Ledo et al. (2002) have investigated the validity of 2D modelling in situations where the structure is in fact 3D. They suggest that measurements made above a structure of finite 2D strike length are best interpreted in 2D using only the TM mode responses.

Pseudosections of the TM mode apparent resistivities and phases are shown in Fig. 2. The apparent resistivity data have been corrected for static-shift (Jones 1988) on the basis of the results of direct current (dc) resistivity soundings and test electromagnetic array profiling (Bostick 1986; Torres-Verdin & Bostick 1992) data in the central part of the transect (von Borstel 2001). These measurements indicate that the near-surface value of resistivity (c. 300 Ωm) is uniform along the transect. The apparent resistivity curves have thus been shifted (e.g., McLoughlin et al. 2002) so that the value of apparent resistivity at the highest frequencies of observation are compatible with this value.

The data show a significant region of low apparent resistivity beneath the southeast part of the transect. This has two main foci of low resistivity: (1) beneath sites H–G, which spans the region between the two fault traces; and (2) to the southeast of site E, where previous measurements (e.g., McLoughlin et al. 2002) indicate that Tertiary sediments underlie the surface gravels. These regions of low apparent resistivity coincide with higher phase values at high frequency which pinch out to the northwest. Higher apparent resistivity and lower phase values beneath the northwest part of the transect are associated with basement greywacke,

although modelling discussed below suggests that the observed apparent resistivity values <100 Ωm beneath site C are underestimates of the true values.

NUMERICAL MODELLING AND INVERSION

As an initial stage in the interpretation of the data, 2D numerical inversion (Smith & Booker 1991) of the static-shift corrected TM mode responses was carried out. The sensitivity of the data to the basic features of the derived structure was then explored through 2D numerical forward modelling. The fit of models to the observed data have been quantified in terms of separate calculations of χ^2 ($= \sum (\text{model value} - \text{observed value})^2 / \text{observed value}$) for the nine periods of variation at which model calculations were performed, for both the \log_{10} of the apparent resistivity (ρ_a) and for phase (ϕ_a) values scaled so that χ^2 misfits in phase and apparent resistivity are equivalent. A 2D resistivity model, which gives the best fit throughout the entire frequency range to the TM mode data ($\chi^2(\rho_a) = 4.13$, $\chi^2(\phi_a) = 3.07$), is shown in Fig. 3. Examples of fits to individual sites are shown in Fig. 4, which also illustrates that uncertainties in the observed data are generally small, the main exception being in some of the phase data at low frequency. The largest misfit to the observed data at a single site is at the most northwestern site C, discussed further below. Misfits to the data at the southeastern sites B and K probably result from degradation of the data at these sites by cultural noise.

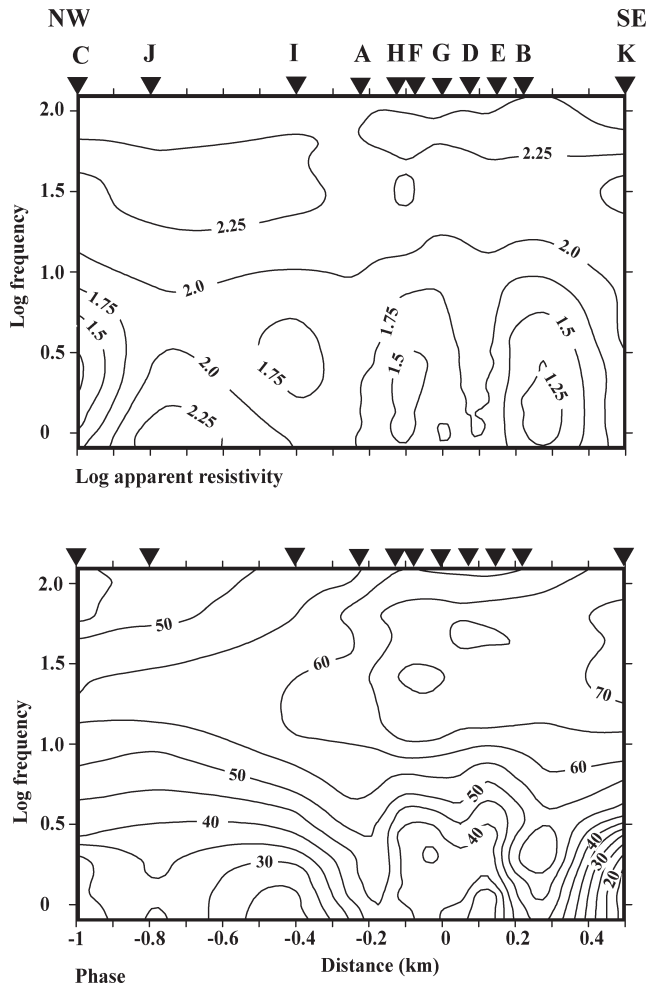


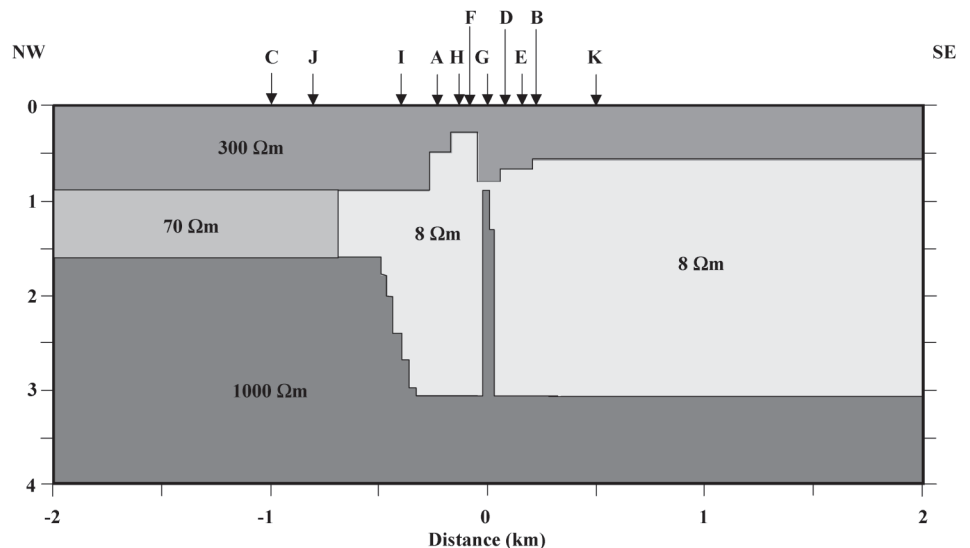
Fig. 2 Pseudosections of measured TM mode apparent resistivity and phase data. Apparent resistivity contours are the $\log_{10}(\rho_a)$; phase (ϕ_a) contours are in degrees.

Testing of the sensitivity of the data to the model shown in Fig. 3 demonstrates that it is difficult to achieve a good fit to the low frequency apparent resistivity data at site G without worsening the fits, particularly to the phase data, at nearby sites H, F, and D. This apparent incompatibility may result from localised topographic effects on the data at site G where the centre of the electrode array was located near the top of the c. 11 m scarp that marks the southeastern fault trace at this location. As a result of this ambiguity, the existence of the narrow high resistivity region beneath site G must be considered questionable. This feature appears in all 2D inversions carried out on the data (von Borstel 2001), yet a forward model in which it is removed and the 8 Ωm layer is continuous gives an improved fit to the apparent resistivity data ($\chi^2(\rho_a) = 3.86$) but a significantly poorer fit ($\chi^2(\phi_a) = 5.65$) to the phase data. Despite the fact that the degree to which this feature is required by the data is uncertain, reasonable geological interpretations of the derived structure are still possible.

The significance of several other features of the model shown in Fig. 3 have also been tested.

- (1) The sharp contrast in resistivity between sites J and I below 1.5 km depth is necessary to give the increase in apparent resistivity at low frequency observed at sites C, J, and I. The underlying dip of this boundary below 1.5 km depth is not well constrained by the data.
- (2) The shallowing to the southeast of the upper surface of the 8 Ωm structure beneath sites A, H, and F is well constrained by the data.
- (3) The modelling of the main low resistivity region as a single resistivity value of 8 Ωm is non-unique. The resistivity of the region beneath sites I–F may be increased up to as much as 30 Ωm with only a slight overall degradation of the fit to the data ($\chi^2(\rho_a) = 5.73$, $\chi^2(\phi_a) = 2.74$). Decreasing the resistivity of the region southeast of site D to 3 Ωm improves the fit at site B.
- (4) The model responses are insensitive to variations in the base of the low resistivity region. It can be inferred that

Fig. 3 Best fitting 2D forward model of resistivity structure across the Wairarapa Fault.



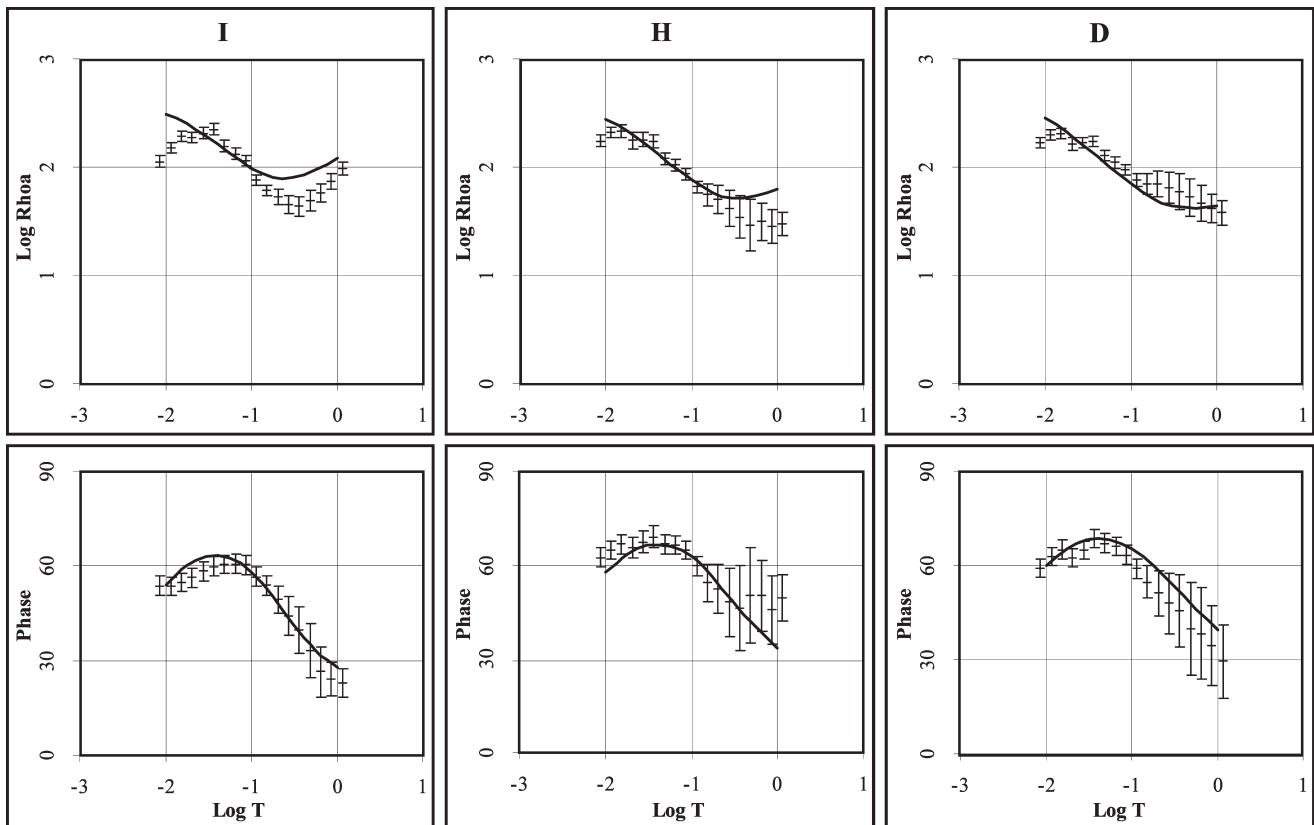


Fig. 4 Fit of the model shown in Fig. 3 to the data are a selection of sites. Apparent resistivities are in Ωm , phase in degrees, and period in seconds.

there is a minimum conductance for this part of the model which gives a satisfactory fit to the data; however, the data do not extend to low enough frequency to resolve the base of the low resistivity zone.

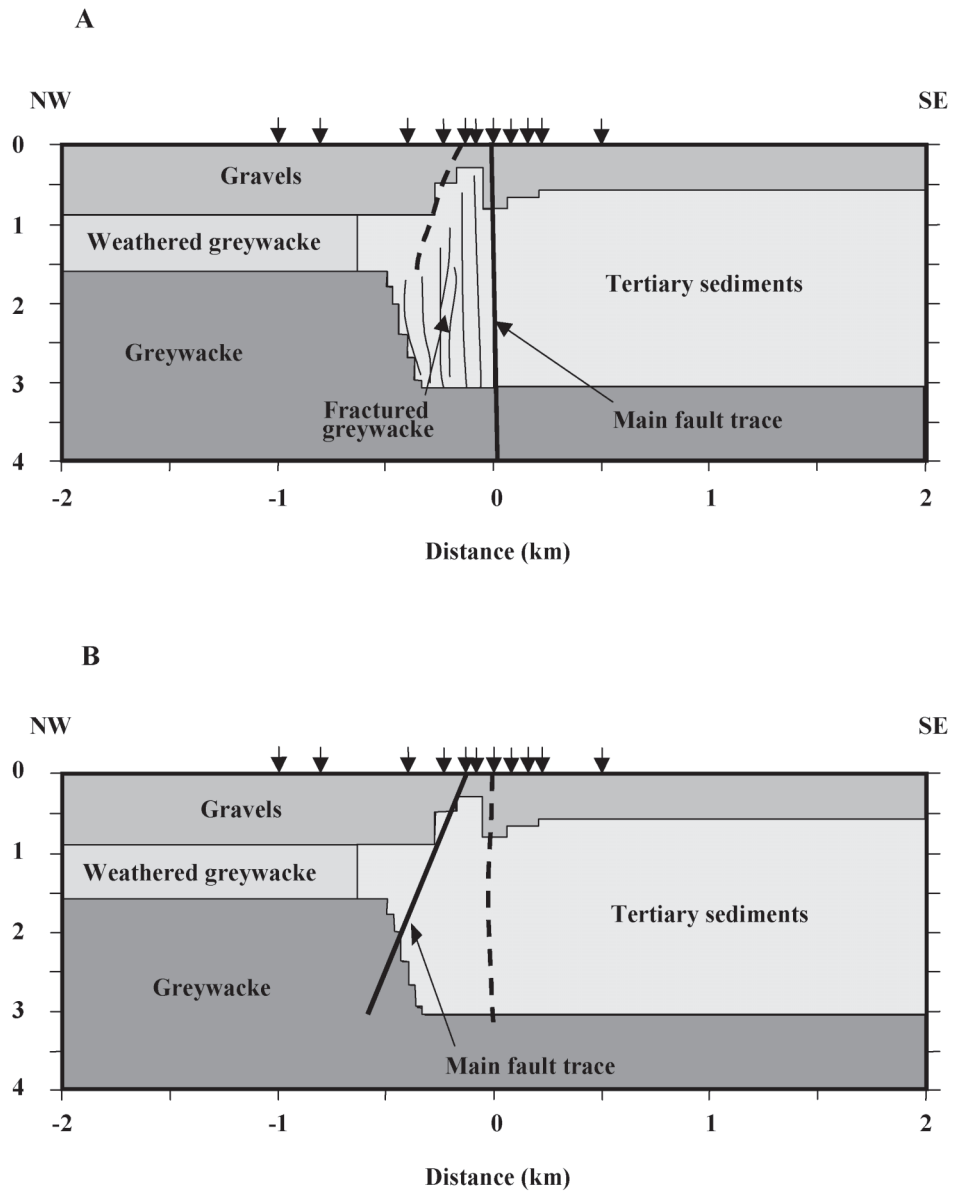
- (5) The layer of $70 \Omega\text{m}$ resistivity and thickness c. 0.7 km beneath sites C and J (interpreted below as weathered greywacke) is resolved only in terms of its conductance (conductivity-thickness product). An equivalent layer of resistivity $100 \Omega\text{m}$ with its upper surface at only 400 m depth fits the data equally well and is in fact more geologically reasonable as the thickness of the overlying gravels to the northwest of the fault is expected to be thinner than to the southeast. The layer is required to attempt to fit the deep minimum in apparent resistivity at site C which occurs at frequencies between 10 and 1 Hz (Fig. 2). In fact, none of the models which have been tested are able to do this satisfactorily. The known geological structure at the northwestern end of the transect (greywacke underlying surface river gravels) is such as to suggest that the apparent resistivity should be expected to show only a slight minimum similar to that seen, for example, at site J (Fig. 2). The 2D modelling results appear to support this expectation. It seems likely, therefore, that the apparent resistivity values at site C, for frequencies lower than 10 Hz , are underestimates of the true values and may reflect the fact that in the frequency range $10\text{--}1 \text{ Hz}$ the natural signal strength is generally very low.

INTERPRETATION AND DISCUSSION

Two possible interpretations of the electrical resistivity structure are possible. The first (shown in Fig. 5A) is based on the model shown in Fig. 3 in which the $8 \Omega\text{m}$ region is split by a narrow region of high resistivity. The interpretation is not, however, dependent on the existence of this feature. In this interpretation, the low resistivity between the two fault traces is inferred to be due to fluid penetration into fractured greywacke between the fault traces. Resistivity values of $<10 \Omega\text{m}$ due to fluid penetration and subsequent alteration in fracture zones have previously been observed on the Apine Fault (Ingham & Brown 1998) and on the San Andreas Fault (Unsworth et al. 1999). In Fig. 5A, fracturing appears to extend somewhat to the northwest of the northwestern of the two traces, while even farther to the northwest the layer of $70 \Omega\text{m}$ resistivity is interpreted to represent weathered greywacke lying beneath the gravels of the Tauwharenikau River valley. To the southeast of site G, the low resistivity is interpreted as being due to the Tertiary sediments underlying the surface gravels. In this interpretation, the location of the main trace of the Wairarapa Fault, that is, the contact at depth between the Tertiary sediments to the southeast and greywacke to the northwest, is between the two conductive zones (i.e., coincident with the resistive finger in Fig 3). The complication of the fracture zone between the two traces of the fault means that the dip of this contact surface cannot be resolved.

An alternative interpretation (Fig. 5B) assumes that the two conductive regions are actually contiguous and are not

Fig. 5 Possible geological interpretations of the 2D resistivity structure shown in Fig. 3.



separated by a resistive strip beneath site G. In this situation, the main trace of the Wairarapa Fault may be correlated with the northwestern of the two fault traces and the entire conductive region with the Tertiary sediments underlying the surface gravels. Fracturing and associated fluid penetration may still occur between the fault traces. The constraint on the southeastwards shallowing of the top of the conductor beneath sites A, H, and F suggests that the fault dips to the northwest. Given the uncertainties in the model, a numerical estimate of the dip is hard to obtain but a value of $80 \pm 10^\circ$ is not unreasonable.

The results suggest that very closely spaced MT measurements may be able to provide detailed images of the electrical structure associated with faults. Use of spacing of as little as 50 m between measurement locations allows the accurate location of lateral resistivity contrasts. In the present case, the image of the electrical structure associated with the Wairarapa Fault zone shows a transition from low resistivity, associated with Tertiary sediments on one side of the fault, to high resistivity greywacke on the other. However,

the data also illustrate the potential difficulties in interpretation which can arise. In this case, fluid penetration into fractured rock has possibly led to a lowering of the bulk electrical resistivity to values which obscure the actual resistivity contrast across the fault zone. This results in two possible interpretations of the derived structure. In contrast, images of either fluid penetrated fault zones where both sides of the fault zone have a similar high resistivity, or, of faults across which the resistivity contrast is not complicated by the presence of fluids, are likely to provide even higher resolution of the separate features (Ingham in press). Exploration of the significance of derived features in such an electrical model clearly have the potential to resolve the nature and dip of fault structures, particularly in the near surface.

ACKNOWLEDGMENTS

The authors acknowledge useful reviews of the manuscript provided by Derek Woodward and an anonymous referee.

REFERENCES

- Bostick, F. X. Jr 1986: Electromagnetic array profiling (EMAP). 56th SEG meeting, Houston, USA. Expanded abstracts. Pp. 60–61.
- Crampin, S.; Volti, T.; Chasin, S.; Gudmundsson, A.; Stefansson, R. 2002: Indication of high pore-fluid pressures in a seismically-active fault zone. *Geophysical Journal International* 151: F1–F5.
- Grapes, R.; Wellman, H. 1988: The Wairarapa Fault. *Research School of Earth Sciences, Geology Board of Studies Publication No. 4*. Wellington, Victoria University of Wellington.
- Hickman, S.; Sibson, R.; Bruhn, R. 1995: Mechanical involvement of fluids in faulting. *Journal of Geophysical Research* 100: 12831–12840.
- Ingham, M. in press: High resolution electrical imaging of fault zones. *Physics of the Earth and Planetary Interiors*.
- Ingham, M. R.; Brown, C. 1998: A magnetotelluric study of the Alpine Fault, New Zealand. *Geophysical Journal International* 135: 542–552.
- Jones, A. G. 1988: Static shift of magnetotelluric data and its removal in a sedimentary environment. *Geophysics* 7: 967–978.
- Jones, A. G.; Kurtz, R. D.; Boerner, D. E.; Craven, J. A.; McNeice, G. W.; Gough, D. I.; DeLaurier, J. M.; Ellis, R. G. 1992: Electromagnetic constraints on strike-slip fault geometry—the Fraser River fault system. *Geology* 20: 561–564.
- Ledo, J.; Queralt, P.; Marti, A.; Jones, A. G. 2002: Two-dimensional interpretation of three-dimensional magnetotelluric data: an example of limitations and resolution. *Geophysical Journal International* 150: 127–139.
- McLoughlin, C.; Ingham, M.; Whaler, C.; McKnight, D. 2002: A magnetotelluric transect of the Wairarapa region, New Zealand. *New Zealand Journal of Geology and Geophysics* 45: 257–269.
- Rice, J. R. 1992: Fault stress states, pore pressure distributions, and the weakness of the San Andreas Fault. In: Evans, B.; Wang, T. F. *ed.* Fault mechanics and transport properties of rocks. San Diego, USA, Academic. Pp. 475–503.
- Schnegg, P.-A.; Le Quang, B. V.; Fischer, G.; Weaver, J. T. 1983: Audiomagnetotelluric study of a structure with a reverse fault. *Journal of Geomagnetism and Geoelectricity* 35: 653–671.
- Schnegg, P.-A.; Fischer, G.; Le Quang, B. V.; Weaver, J. T. 1986: Investigation of a buried vertical fault with natural and controlled source AMT. *Annales Geophysicae* 4: 139–144.
- Sibson, R.; Robert, F.; Poulsen, K. H. 1988: High-angle reverse faults, fluid-pressure cycling, and mesothermal gold-quartz deposits. *Geology* 16: 551–555.
- Smith, J. T.; Booker, J. R. 1991: Rapid inversion of two- and three-dimensional magnetotelluric data. *Journal of Geophysical Research* 96: 1168–1171.
- Torres-Verdin, C.; Bostick, F. X. Jr 1992: Principles of spatial surface electric field filtering in magnetotellurics: electromagnetic array profiling (EMAP). *Geophysics* 57: 603–622.
- Unsworth, M.; Egbert, G.; Booker, J. 1999: High-resolution electromagnetic imaging of the San Andreas fault in central California. *Journal of Geophysical Research* 104: 1131–1150.
- von Borstel, O. I. 2001: The structure of the Wairarapa Fault as obtained from magnetotelluric soundings and electromagnetic array profiling (EMAP). Unpublished BSc Hons thesis, School of Earth Sciences, Victoria University of Wellington, Wellington, New Zealand.
- Wannamaker, P. E. 1999: Affordable magnetotellurics: interpretation in natural environments. In: Orastaglio, M.; Spies, B. *ed.* Three-dimensional electromagnetics. *Geophysical Developments Series* 7. Tulsa, Society of Exploration Geophysicists. 724 p.